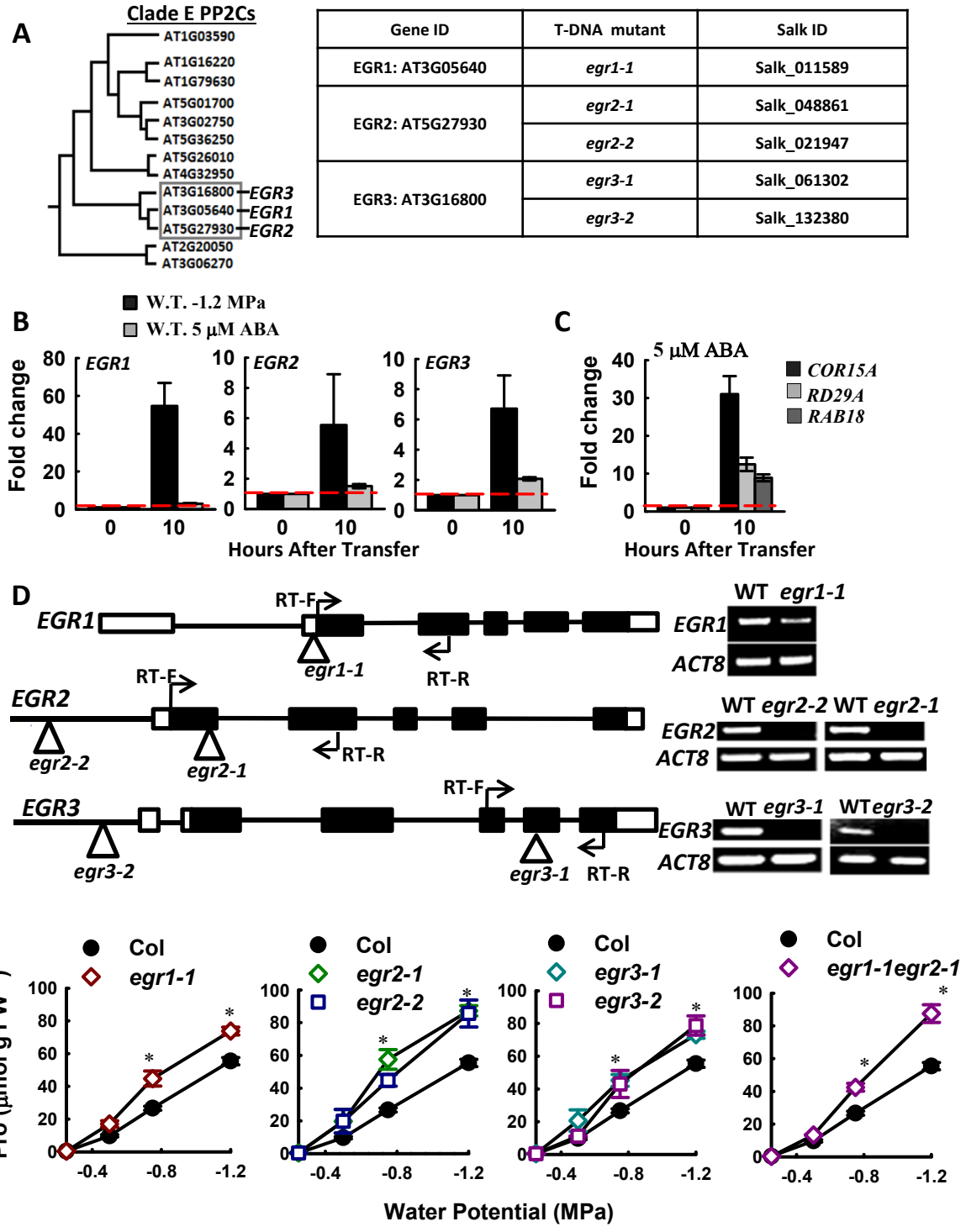

Gene ID	T-DNA mutant	Salk ID
EGR1: AT3G05640	*egr1-1*	Salk_011589
EGR2: AT5G27930	*egr2-1*	Salk_048861
	egr2-2	Salk_021947
EGR3: AT3G16800	*egr3-1*	Salk_061302
	egr3-2	Salk_132380

Figure S1

Supplemental Figure S1: *Clade E Growth-Regulating* (*EGR*) PP2C mutants, gene expression and proline accumulation.

A. Phylogenetic tree of the Clade E PP2Cs showing the three EGRs examined in this study. Tree is based on Schweighofer et al. (2004). At right is a list of EGR T-DNA mutants used in this study. Gray box shows location of EGRs on the phylogenetic tree.
B. Exogenous ABA has minimal effect on *EGR* gene expression. *EGR* expression was measured under control conditions (time 0) or 10 h after transfer of Col wild type to plates containing 5 micromolar ABA or low water potential PEG-agar plates (-1.2 MPa). Data are means ± S.E. (n = 6) combined from two independent experiments. Note that the stress data are the same as in Figure 1A and are shown here for comparison to the ABA treatment. Dashed red line shows the gene expression level in the control (1-fold change).
C. Expression of ABA-induced marker genes in Col wild type shows that the 5 micromolar ABA treatment used in B was sufficient to induced expression of ABA-regulated genes. Dashed red line shows the gene expression level in the control (1-fold change).
D. T-DNA insertion sites and RT-PCR analysis of EGR T-DNA lines. Note that *egr2* and *egr3* physiology data in Figure 1B are the combined data from *egr2-1* and *egr2-1* or *egr3-1* and *egr3-2*, respectively. The insertion site of *egr1-1* near the translational start site (along with transgenic complementation of *egr1-1*, see main text) suggests that the T-DNA insertion blocks EGR1 translation even though EGR1 mRNA can still be detected. RT-F and RT-R shows the positions of the primers used for RT-PCR to check *EGR* expression in the mutants. The RT-PCR was performed on two biological replicates from separate experiments with essentially identical results.
E. Proline accumulation across a range of water potentials on PEG-agar plates. Proline was measured 96 h after transfer of seedlings to the indicated water potentials. Data are means ± S.E. (n = 4-8) combined from two independent experiments. Significant differences from wild type ($p \leq 0.05$ by T-test) are indicated (*).

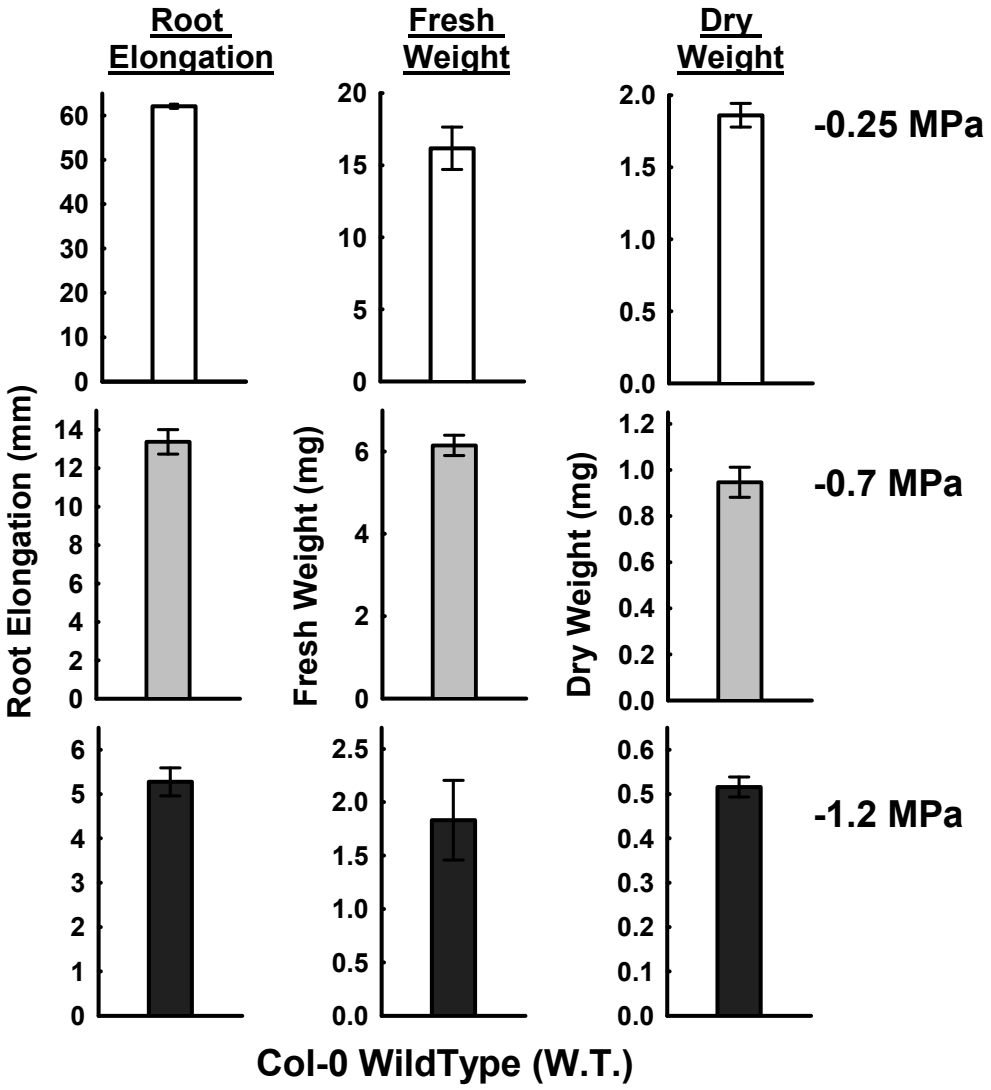

Supplemental Figure S2: Seedling growth measurements of Col-0 wild type in control as well as -0.7 and -1.2 MPa low ψ_w treatments.
Absolute growth values of Col-0 wild type (W.T.) for experiments shown in the main text where mutant and transgenic growth data were normalized to the Col-0 W.T. Five-day-old seedlings were transferred to the indicated treatments and root elongation, fresh weight and dry weight measured 10 days later for the stress treatments and 7 days later for the unstressed control (-0.25 MPa). Data are means ± S.E. (n > 100 for root elongation and n > 25 for fresh and dry weight) combined from multiple independent experiments.

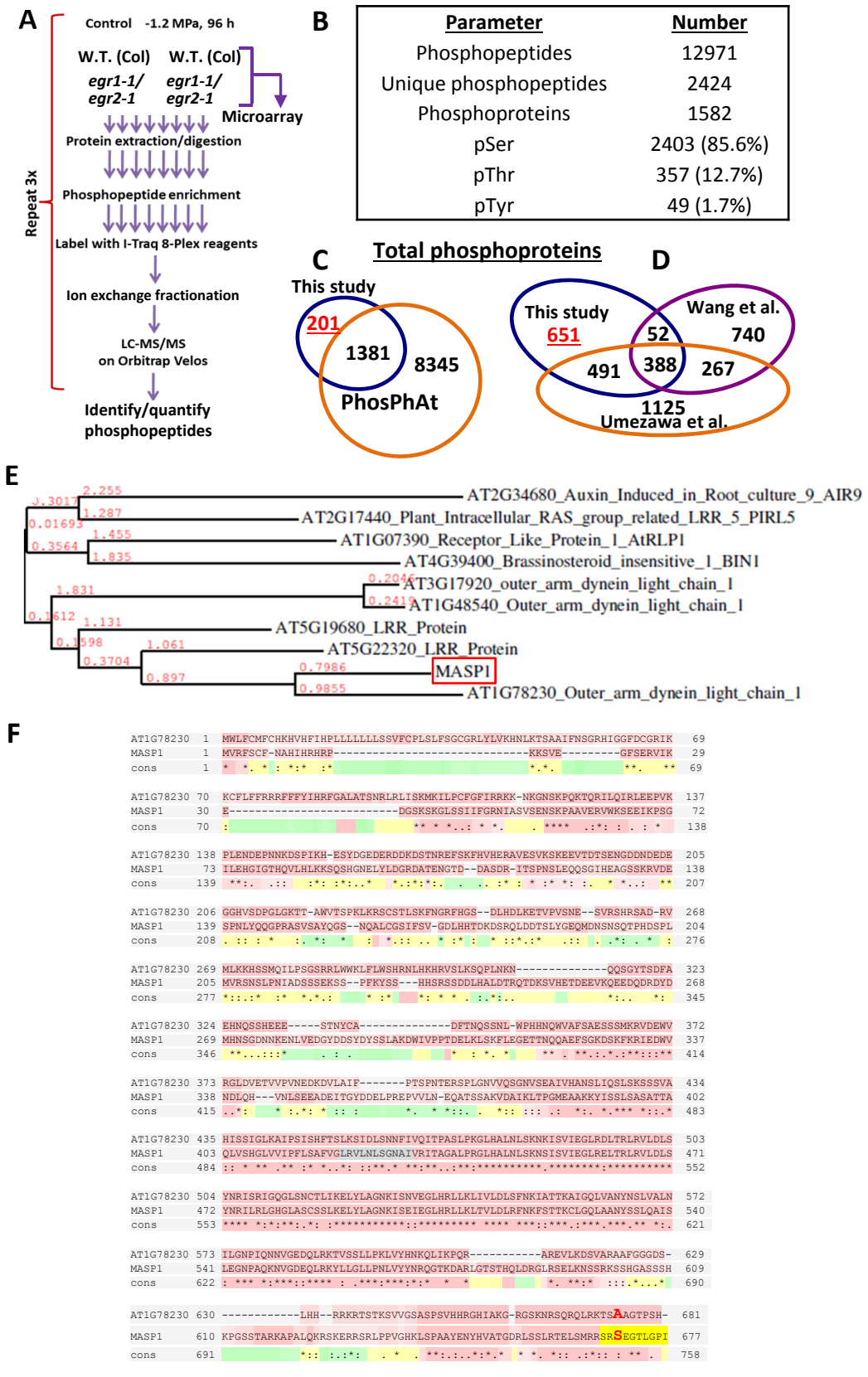
A
Control -1.2 MPa, 96 h
W.T. (Col)
egr1-1/ egr2-1
W.T. (Col)
egr1-1/ egr2-1
Microarray
Protein extraction/digestion
Phosphopeptide enrichment
Label with I-Traq 8-Plex reagents
Ion exchange fractionation
LC-MS/MS on Orbitrap Velos
Identify/quantify phosphopeptides
Repeat 3x
B
Parameter
Number
Phosphopeptides
12971
Unique phosphopeptides
2424
Phosphoproteins
1582
pSer
2403 (85.6%)
pThr
357 (12.7%)
pTyr
49 (1.7%)
C
Total phosphoproteins
This study
201
1381
8345
PhosPhAt
D
This study
651
Wang et al.
52
740
491
388
267
1125
Umezawa et al.
E
AT2G34680_Auxin_Induced_in_Root_culture_9_AIR9
AT2G17440_Plant_Intracellular_RAS_group_related_LRR_5_PIRL5
AT1G07390_Receptor_Like_Protein_1_AtRLP1
AT4G39400_Brassinosteroid_insensitive_1_BIN1
AT3G17920_outer_arm_dynein_light_chain_1
AT1G48540_Outer_arm_dynein_light_chain_1
AT5G19680_LRR_Protein
AT5G22320_LRR_Protein
MASP1
AT1G78230_Outer_arm_dynein_light_chain_1
F
AT1G78230
MASP1
cons

Figure S3

Supplemental Figure S3: Phosphoproteomic analysis of drought acclimation identifies new aspects of the stress phosphoproteome including Microtubule Associated Stress Protein 1 (MASP1).

A. Diagram of the phosphoproteomic and microarray procedure.
B. Summary of phosphopeptides identified and portion of phosphoserine, threonine and tyrosine.
C. Comparison of phosphoproteins listed in the PhosPhAt database (http://phosphat.uni-hohenheim.de/) to proteins identified in our study. More than twelve percent of the phosphoproteins identified in our study were not listed in PhosPhAt (indicated by the red underlined number).
D. Comparison of phosphoproteins identified in our study of longer term (96 h) low water potential treatment versus previous studies of short term (90 minutes or less) ABA or dehydration treatments (Wang et al., 2013; Umezawa et al., 2013). 651phosphoproteins were unique to our dataset (indicated by the red underlined number). The list of phosphopeptides identified in our study, along with comparison to these previous studies, can be found in Supplementary Dataset S4. Note that for phosphoproteins identified in multiple studies, the phosphorylation sites identified may differ between the different datasets.
E. MASP1 (At4g03260) homologues: The 10 Arabidopsis proteins most similar to MASP1 (based on protein BLAST search) were used to construct a phylogentic tree. The tree was constructed using the phylogeny.fr web service without use of Gblocks analysis. Red numbers indicate the phylogenetic distance between proteins and the red box indicates MASP1. Sequences and alignments used to generate this tree are given in Supplemental Dataset 11).
F. Sequence alignment of MASP1 and its nearest homolog (At1g78320). The MASP1 phosphopeptide found in our analysis is highlighted (yellow) and the MASP1 phosphorylation site indicated by the enlarged red font. Note that despite the high similarity of the C-terminal region, the MASP1 phosphorylation site at S670 is not conserved in At1g78320.

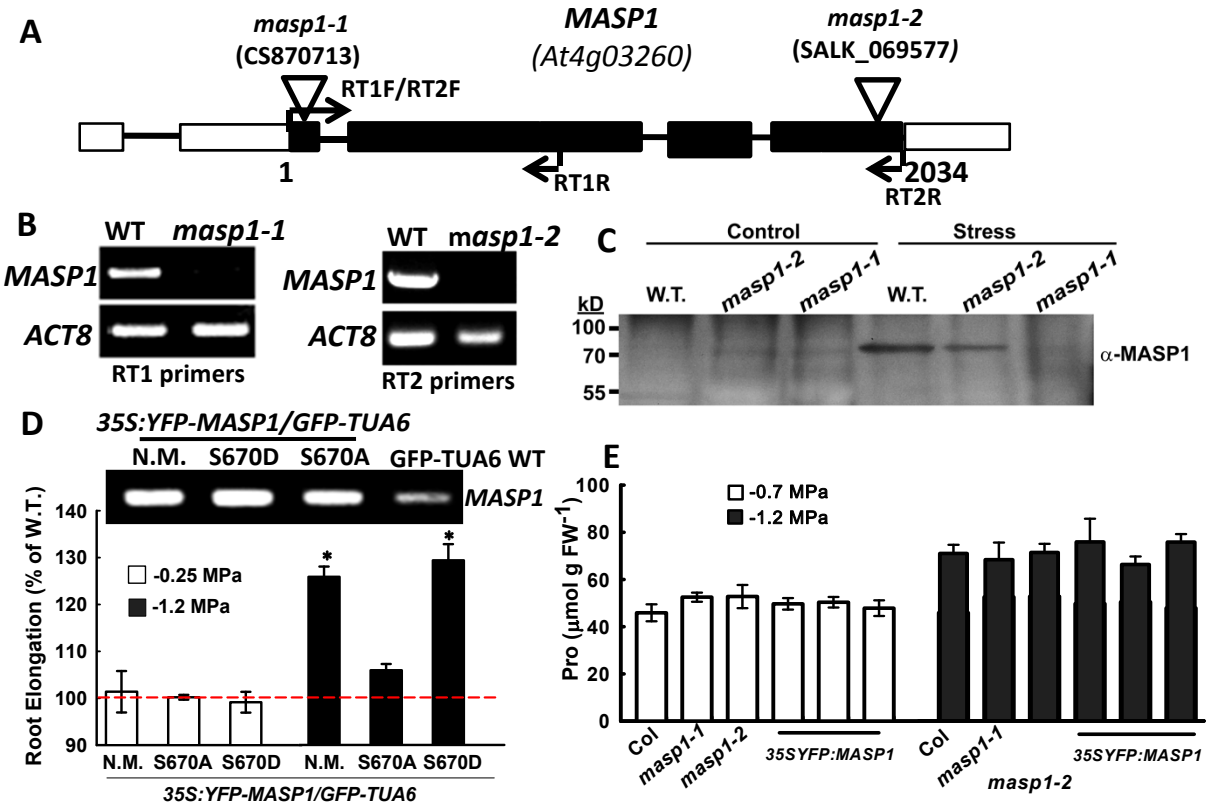

Supplemental Figure S4: MASP1 T-DNA lines, proline accumulation and expression of MASP1 in the GFP-TUA6 background.

A. T-DNA insertions sites of *masp1-1* and *masp1-2*. Black bars indicate the coding regions, lines indicate introns and white bars indicate untranslated regions. Triangles indicate T-DNA insertion sites and arrows indicate direction of amplification from the primers shown.

B. RT-PCR verifies that both *masp1-1* and *masp1-2* lack full length *MASP1* transcript.

C. Immunoblot showing that *masp1-1* completely lacks MASP1 protein. *masp1-2* still produces a reduced level of protein; however, the position of the T-DNA insertion site indicates that this is truncated protein or has altered amino acid sequence at the C-terminal end including loss of the S670 phosphorylation site. MASP1 protein level was low and could not be detected in unstressed plants but could be detected after stress treatment (96 h, -1.2 MPa). The predicted molecular weight of MASP1 is 74.7 kD.

D. Verification of *Pro35S:MASP1* expression and phenotype in the GFP-TUA6 background used for microtubule analysis. RT-PCR showed that each form of *MASP1* was expressed at essentially the same level in the transgenic lines. Increased root elongation was observed in GFP-TUA6 plants expressing unmutated *35S:MASP1 N.M. (N.M. = No Mutation)* or MASP1^{S670D} *(*phosphomimic) while MASP1^{S670A} (phosphonull) had less effect, consistent with the phenotypes of *35S:YFP-MASP1* transgenics. Data are means of ± S.E. and are combined data of two independent lines for each construct. (* indicates $p \leq 0.05$ compared to wild type by T-test). Dashed red line indicates the wild type level of root elongation.

E. MASP1 does not affect low water potential-induced proline accumulation.
Proline accumulation was measured 96 h after transfer of seedlings to either -0.7 MPa or -1.2 MPa. Data are means ± S.E. (n = 4-6). No significant difference in proline accumulation compared to wild type was observed for either *masp1* mutants or *MASP1* overexpression lines. The same three independent *MASP1* overexpression lines were analyzed for proline accumulation and growth phenotypes shown in the main text.

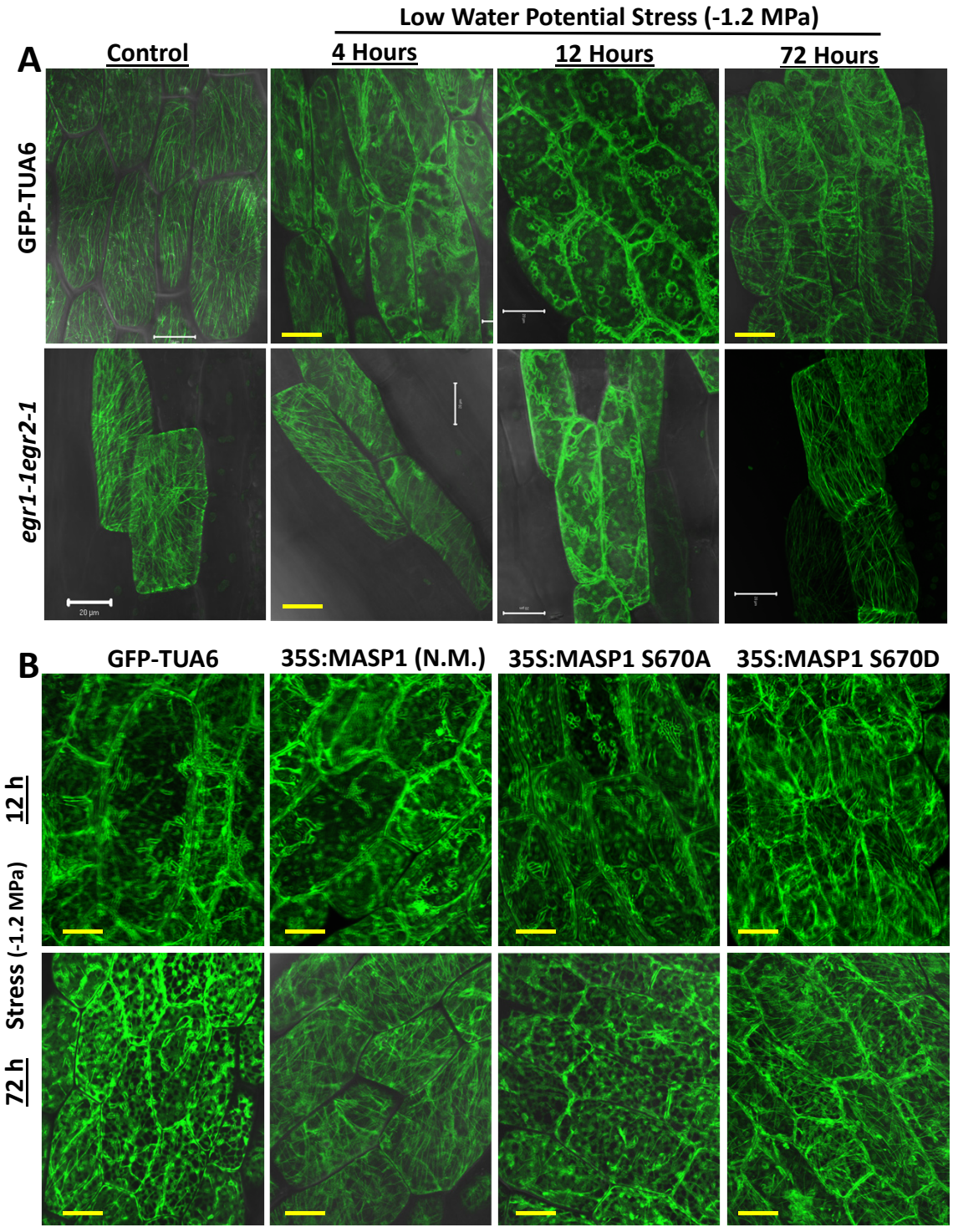
A
Low Water Potential Stress (-1.2 MPa)
Control
4 Hours
12 Hours
72 Hours
GFP-TUA6
egr1-1egr2-1
B
GFP-TUA6
35S:MASP1 (N.M.)
35S:MASP1 S670A
35S:MASP1 S670D
12 h
Stress (-1.2 MPa)
72 h

Figure S5

Supplemental Figure S5: Time course of MT structure in wild type (GFP-TUA6), *egr1-1 egr2-1* and MASP1 overexpression lines after transfer from control (-0.25 MPa) to low ψ_w stress (-1.2 MPa).

A. Time course analysis of MT in GFP-TUA6 (wild type) and *egr1-1 egr2-1*. Both lines had loss of MT organization at 12 h. *egr1-1 egr2-1* had more extensive MT recovery at 72 h and may also have had slower loss of MT organization in the first hours of stress (4 h).

B. MASP1 overexpression lines in the GFP-TUA6 background imaged at 12 and 72 h after transfer to -1.2 MPa stress. All lines had near total loss of cortical MT organization at 12 h. Lines with overexpression of MASP1 N.M. (No Mutation at the phosphorylation site) and phosphomimic MASP1 (S670D) started to have more extensive MT recovery by 72 h.

For both A and B, seven-day-old seedlings were imaged by confocal microscopy at the indicated times after transfer. Images are from cells at the base of the hypocotyl elongation zone. Scale bars = 20 micrometers.

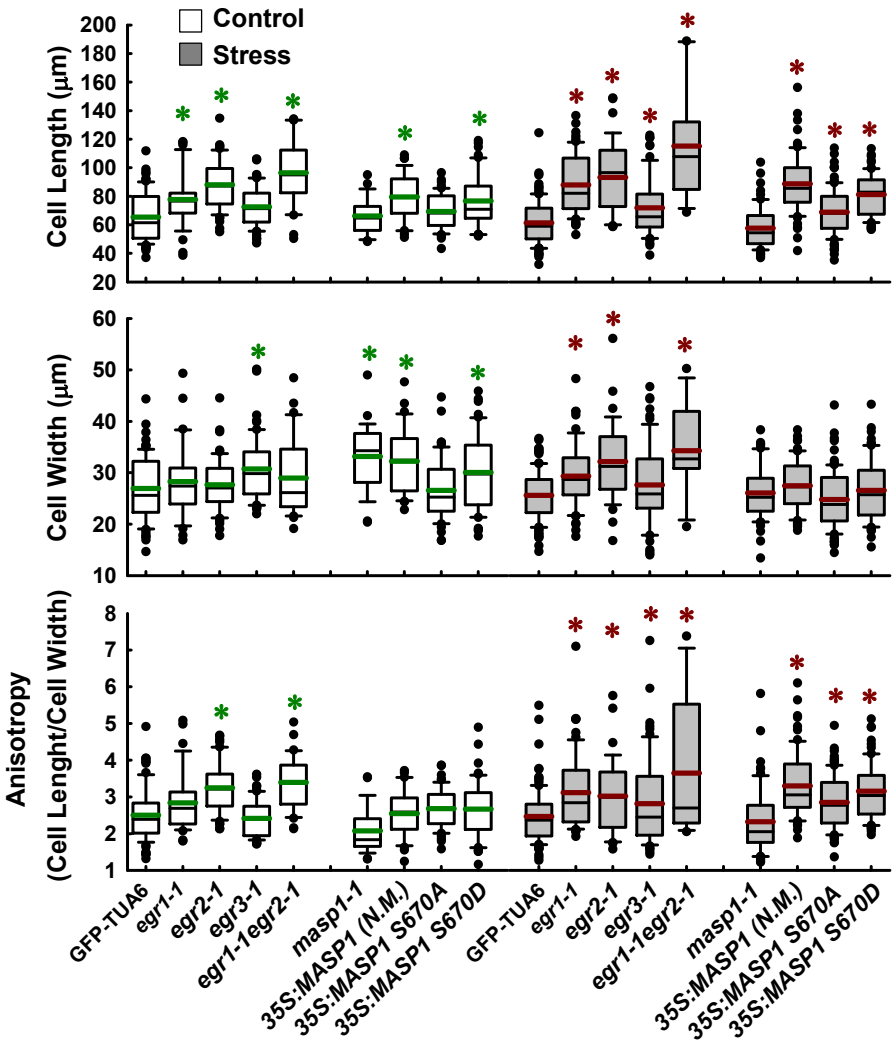

Supplemental Figure S6: Cell size and anisotropy of *EGR* and *MASP1* mutant and overexpression lines.

Cell size measurements were conducted on the same cells at the end of the hypocotyl elongation zone that were used for microtubule analysis. Anisotropy was calculated from the length/width ratio of individual cells. Data are means ± S.E. (n = 20 to 60) of cells from multiple seedlings. * indicates significant difference ($p \leq 0.05$ by T-test) compared to wild type in the same treatment. Boxes show the 25-75 percentiles of the data, bars show the 5-95 percentile and black circles show outlier data points. Black lines in the boxes are the mean while green or red lines are the median of the data.

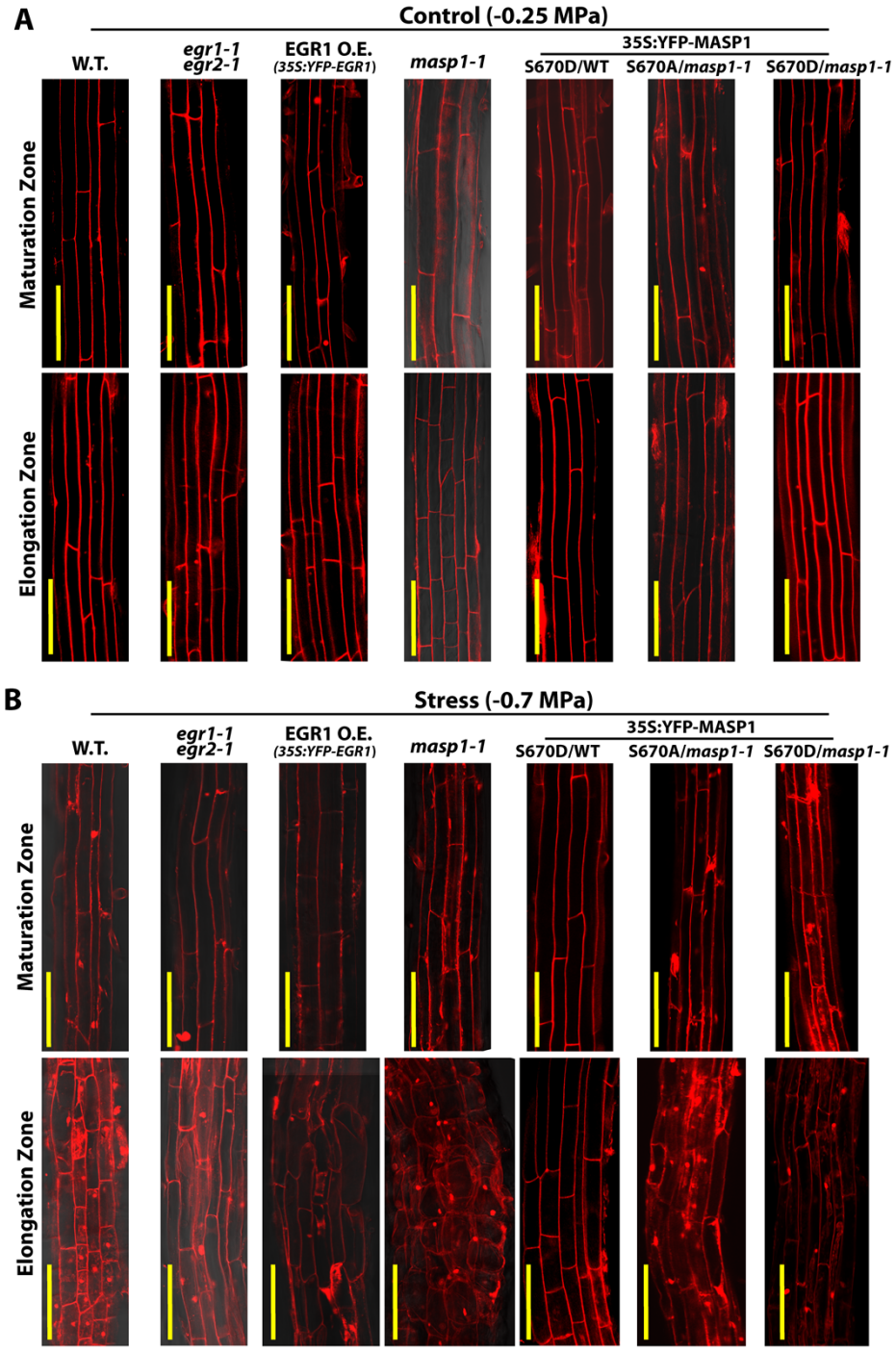

Supplemental Figure S7: Propidium Iodide (PI) staining of root cells of *EGR* and *MASP1* mutant and overexpression lines.

Cells in the root elongation zone or maturation zone were stained at 96 h after transfer to the indicated treatments. Note that for the stress treatment, the maturation zone cells had completed growth before transfer to the stress and were thus less affected than elongation zone cells. Both *EGR1* overexpression (O.E.) and *masp1-1* had disrupted cell expansion and anisotropic swelling in the stress treatment. Note that stress treatment of -0.7 MPa was used as -1.2 MPa can cause cell damage which interferes with PI staining. Scale bars = 100 micrometers.

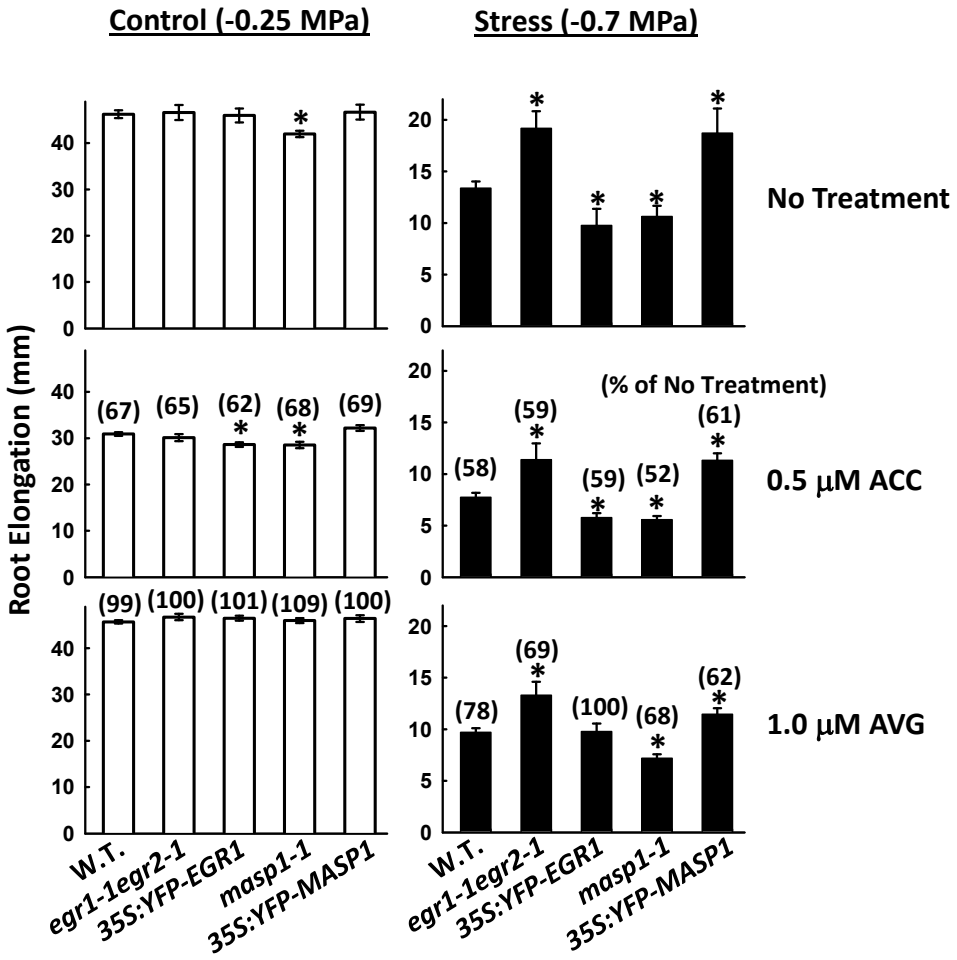

Supplemental Figure S8: Effect of ACC and AVG on root elongation of *EGR* and *MASP1* mutant and overexpression lines.

Five-day-old seedlings were transferred to the indicated treatments and root elongation over the subsequent 7 days (control) or 10 days (stress) measured. Data are means ± S.E. (n = 5-30) combined from two independent experiments. Asterisks (*) indicate a significant difference ($p \leq 0.05$) compared to wild type in the same treatment. Numbers in parentheses indicate the percent root elongation relative to the same genotype without ACC or AVG (No Treatment).

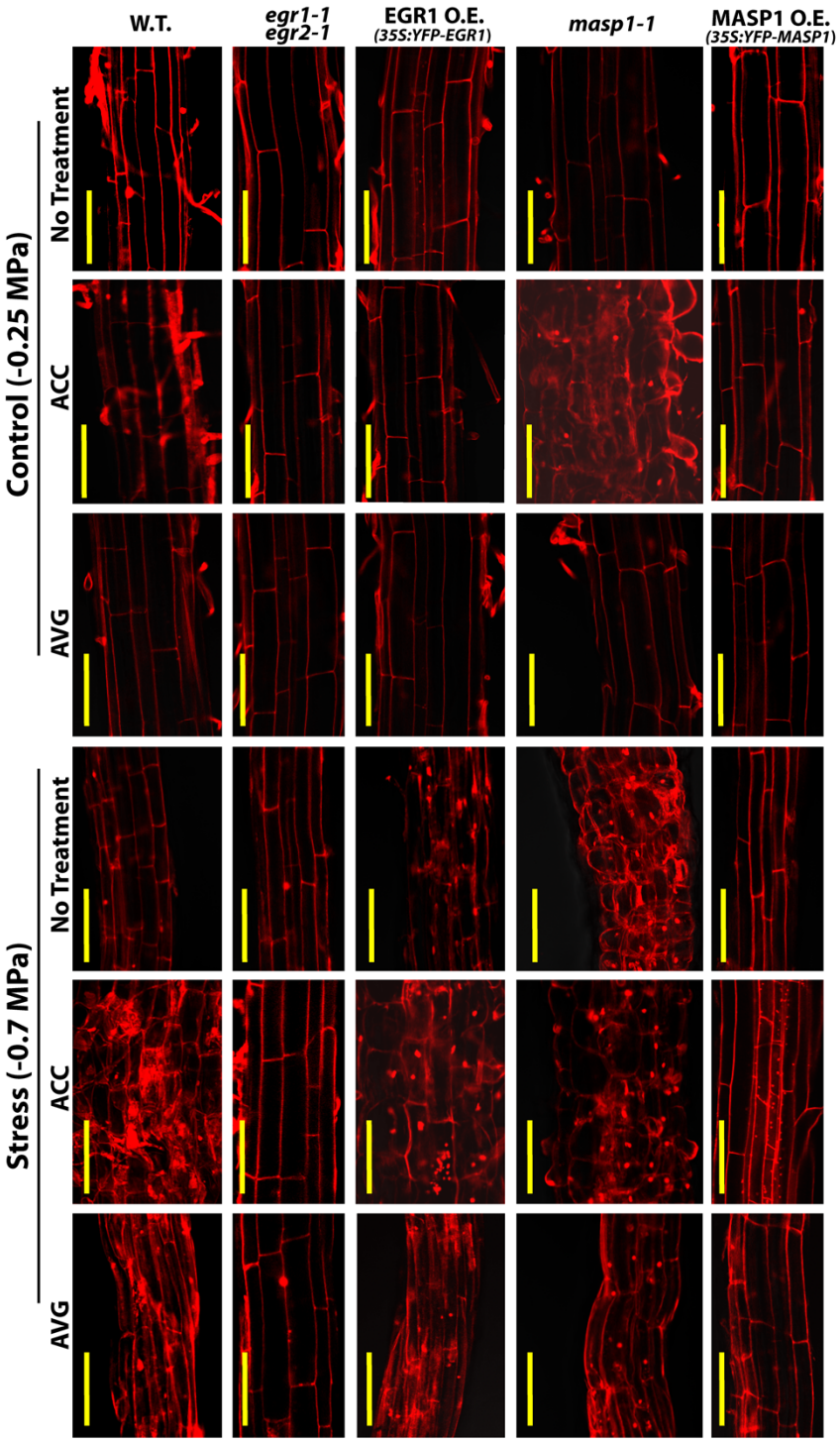

Supplemental Figure S9: Propidium iodide (PI) staining of *EGR* and *MASP1* mutant and overexpression lines after ACC or AVG treatment at high or low ψ_w.
PI staining of the root elongation zone was conducted as described for Supplemental Figure S7 for seedlings collected during the ACC and AVG experiments shown in Figure S8. Loss of MASP1 activity in *masp1-1*, and to a lesser extent EGR1 overexpression (O.E.), increased sensitivity of root cell swelling to ACC, especially at low ψ_w (-0.7 MPa). Conversely, *egr2-1* and *MASP1* O.E. were less sensitive to the induction of root swelling by ACC. AVG could reverse the root swelling but did not completely restore normal cell morphology at low ψ_w. 0.5 μM ACC or 1.0 μM AVG was applied for 7 days (control) or 10 days (stress). Scale bars = 100 μm.

A

I-Tasser
(Top model predicted; C-score = -1.75)

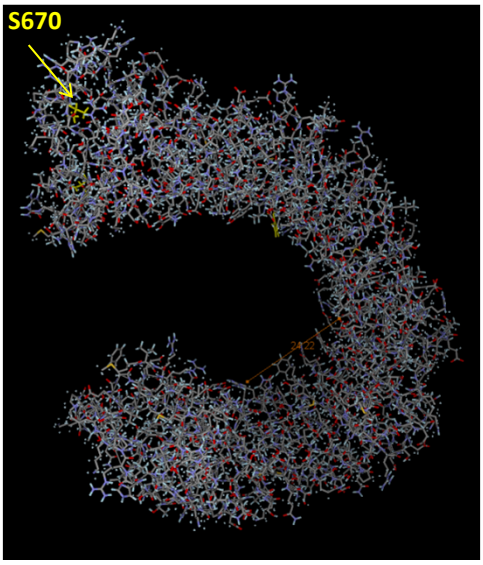

Phyre2
Intensive Mode, 663 residues (98%) modelled at >90% accuracy

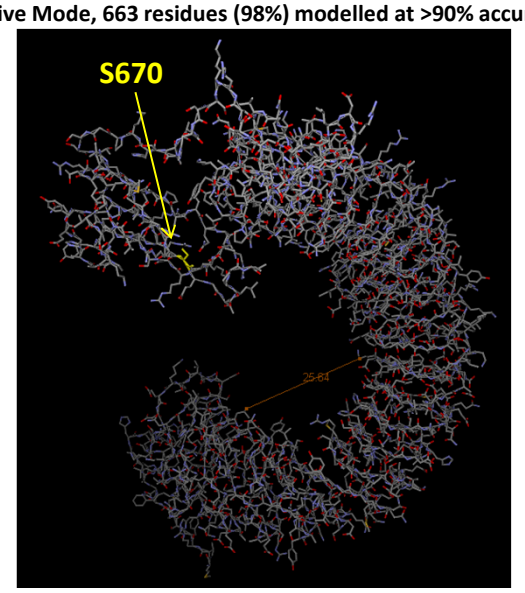

B

MVRFSCFNAHIHRHRPKKSVEGFSERVIKEDGSKSKGLSSIIFGRNIASVSENSKPAAVERVWKSEEIKPSGILEHGIGTHQVLHLKKSQSHGNELYLD
GRDATENGTDDASDRITSPNSLEQQSGIHEAGSSKRVDESPNLYQQGPRASVSAYQGSNQALCGSIFSVGDLHHTDKDSRQLDDTSLYGEQMDN
SNSQTPHDSPLMVRSNSLPNIADSSSEKSSPFKYSSHHSRSSDDLHALDTRQTDKSVHETDEEVKQEEDQDRDYDMHNSGDNNKENLVEDGY
DDSYDYSSLAKDWIVPPTDELKLSKFLEGETTNQQAEFSGKDSKFKRIEDWVNDLQHVNLSEEADEITGYDDELPREPVVLNEQATSSAKVDAIK
LTPGMEAAKKYISSLSASATTAQLVSHGLVVIPFLSAFVGLRVLNLSGNAIVRITAGALPRGLHALNLSKNSISVIEGLRELTRLRVLDLSYN
RILRLGHGLASCSSLKELYLAGNKISEIEGLHRLLKLTVLDLRFNKFSTTKCLGQLAANYSSLQAISLEGNPAQKNVGDEQLRKYLLGLLP
NLVYYNRQGTKDARLGTSTHQLDRGLRSELKNSSRKSSHGASSSHKPGSSTARKAPALQKRSKERRSRLPPVGHKLSPAAYENYHVATGDRLSS
LRTELSMRRSR(pS)EGTLGPI

C

Top 10 threading templates used by I-Tasser

Rank	PDB Hit	Iden1	Iden2	Cov	Norm. Z-score
1	2z64A	0.14	0.18	0.83	1.93
2	1m9sA	0.25	0.14	0.33	1.75
3	2omuA	0.13	0.16	0.64	2.41
4	4mn8A	0.16	0.23	0.83	1.20
5	4fmzA	0.14	0.10	0.48	0.82
6	2omzA	0.16	0.17	0.60	2.79
7	3zyjA	0.16	0.14	0.54	1.15
8	4mn8A	0.14	0.23	0.77	2.96
9	2omzA	0.15	0.17	0.67	1.86
10	3wn4A	0.16	0.23	0.97	1.18

1. Crystal structure of mouse TLR4 and mouse MD-2 complex (lipopolysaccharide binding)
2. Crystal structure of Internalin B (InlB), a Listeria monocytogenes virulence protein containing SH3-like domains. (glycosaminoglycan binding)
3. Crystal structure of InlA (Internalin) G194S+S Y369S/hEC1 complex
4. Crystal structure of flg22 in complex with the FLS2 and BAK1 ectodomains
5. Crystal structure of an internalin (inlF) from Listeria monocytogenes str. 4b F2365 at 1.91 A resolution
6. Crystal structure of InlA (Internalin) Y369A/hEC1 complex
7. NETRING1 IN COMPLEX WITH NGL1 (neuroprotein involved in cell surface interaction)
8. Crystal structure of flg22 in complex with the FLS2 and BAK1 ectodomains
9. Crystal structure of InlA (Internalin) Y369A/hEC1 complex
10. Crystal structure of human TLR8 in complex with DS-877

Top 10 structural analogs in PDB

Rank	PDB Hit	TM-score	RMSD[a]	IDEN[a]	Cov
1	2z64A	0.830	1.01	0.139	0.839
2	3fxiB	0.781	2.57	0.130	0.839
3	3j0aA	0.761	3.88	0.110	0.863
4	3t6qA	0.732	3.47	0.115	0.821
5	3b2dA	0.716	3.87	0.111	0.823
6	3rg1A	0.713	3.70	0.111	0.811
7	3wn4A	0.677	5.16	0.113	0.841
8	3ciyB	0.674	4.92	0.131	0.826
9	3wpbA	0.661	5.00	0.122	0.821
10	2a0zA	0.657	5.18	0.111	0.821

1. Crystal structure of mouse TLR4 and mouse MD-2 complex (with lipopolysaccharide-like ligand).
2. Crystal structure of the human TLR4-human MD-2-E.coli LPS Ra complex Toll-like receptor 5 (lipopolysaccharide ligand)
3. Homology model of human Toll-like receptor 5.
4. Crystal structure of mouse RP105/MD-1 complex (lipopolysaccharide binding complex)
5. Crystal structure of human RP105/MD-1 complex (lipopolysaccharide binding complex)
6. Crystal structure of the RP105/MD-1 complex (lipopolysaccharide binding complex)
7. Crystal structure of human TLR8 in complex with DS-877
8. Mouse Toll-like receptor 3 ectodomain complexed with double-stranded RNA
9. Crystal structure of horse TLR9 (unliganded form)
10. The molecular structure of toll-like receptor 3 ligand binding domain

Figure S10

Supplemental Figure S10: MASP1 structure predicted by I-Tasser and Phyre2 and structural features putatively related the microtubule binding.

A. Predicted MASP1 structures from I-Tasser and Phyre2 both show that MASP1 forms a hook-like shape with the inner diameter of the hook (25-30 nm) compatible with microtubule diameter (microtubule outer diameter is approximately 25 nm) while both the N-terminus and C-terminus (with S670) project away from the central hook.
B. MASP1 amino acid sequence color coded to show position of structural domains: green indicates loop regions, red indicates helix regions and yellow indicates beta-sheet. In addition, analysis of MASP1 by LRRsearch identified six LRR domains (underlined). The phosphorylation site (S670) and phosphopeptide identified in our analysis are shown in purple and italicized.
C. The top templates used by I-Tasser in the prediction of MASP1 structure as well as the top 10 structural analogs. For structural analogs TM score greater than 0.5 indicates a model of correct topology while larger RMSD indicates more local deviation between the MASP1 structural model and the structural analog. It is of interest to note that the majority of the top templates and structural orthologues are proteins involved in cell surface interaction (Internalin for example) or binding to lipopolysaccharide molecules (MD-1 and MD-2).

References

Schweighofer, A., Hirt, H., and Meskiene, L. (2004). Plant PP2C phosphatases: emerging functions in stress signaling. Trends in Plant Science 9, 236-243.

Umezawa, T., Sugiyama, N., Takahashi, F., Anderson, J.C., Ishihama, Y., Peck, S.C., and Shinozaki, K. (2013). Genetics and Phosphoproteomics Reveal a Protein Phosphorylation Network in the Abscisic Acid Signaling Pathway in Arabidopsis thaliana. Science Signaling 6, 270.

Wang, P.C., Xue, L., Batelli, G., Lee, S., Hou, Y.J., Van Oosten, M.J., Zhang, H.M., Tao, W.A., and Zhu, J.K. (2013). Quantitative phosphoproteomics identifies SnRK2 protein kinase substrates and reveals the effectors of abscisic acid action. Proceedings of the National Academy of Sciences of the United States of America 110, 11205-11210